Desalination and Water Treatment
www.deswater.com
doi: 10.5004/dwt.2021.27258

226 (2021) 251–262
June

Adsorption of Pb(II) from aqueous solutions by montmorillonite/Fe_3O_4 nanoparticles: batch and column studies

Mohammad Hadi Mehdinejad[a], Farshad Hamidi[a], Yones Katoki[a], Yousef Dadban Shahamat[a], Ali Parvizimehr[b], Nezamaddin Mengelizadeh[b,*]

[a]*Environmental Health Research Center, Department of Environmental Health Engineering, School of Health, Golestan University of Medical Sciences, Gorgan, Iran*
[b]*Research Center of Health, Safety and Environment, Department of Environmental Health Engineering, Faculty of Evaz Health, Larestan University of Medical Sciences, Larestan, Iran, Tel. +98-939-231-2472; email: nezam_m2008@yahoo.com (N. Mengelizadeh)*

Received 12 April 2020; Accepted 21 March 2021

ABSTRACT

In the present study, magnetic montmorillonite (MMT/Fe_3O_4) was prepared using chemical precipitation for adsorption of Pb(II) and was characterized by scanning electron microscopy, transmission electron microscopy, thermogravimetric analysis, X-ray diffraction and Fourier-transform infrared spectroscopy (FTIR). The results showed that Fe_3O_4 uniformly occurred on MMT. The maximum adsorption capacity of Pb(II) by MMT/Fe_3O_4 was obtained to be 36.76 mg/g, which was higher than the Fe_3O_4 and MMT alone. The removal efficiency of Pb(II) was strongly dependent on the operating factors, where the maximum efficiency occurred at pH of 5, adsorbent dose of 0.4 g/L, Pb(II) concentration of 30 mg/L, stirring rate of 300 rpm, and contact time of 120 min. The adsorption data followed the Langmuir isotherm, and the kinetic results showed that the chemisorption process is the dominant mechanism for Pb(II) removal. The results of the FTIR analysis explained that the Al–OH and Fe–O functional groups have high participation in pollutant adsorption. The column study emphasized that MMT/Fe_3O_4 nanocomposite has excellent efficiency in the treatment of real wastewater containing Pb(II). In addition, excellent magnetic separation and regeneration performance indicated the applicability of adsorbent for the treatment of synthetic and real solutions.

Keywords: MMT/Fe_3O_4; Pb(II); Column study; Adsorption; Removal mechanism

1. Introduction

In recent decades, the presence of heavy metals in aquatic environments has been recognized as an environmental concern due to accumulation in the food chain, high toxicity, and non-degradability. In addition, the presence of these minerals in surface and groundwater contaminated with industrial wastewater has caused human health problems such as cancers [1,2]. Lead (Pb) is one of the most common heavy metals that is continually releasing into the environment from mining, automobile exhaust, coal, electronic waste, and industries [3]. It is toxic and non-degradable and can therefore cause serious health risks such as damage to the nervous system, interference with haemoglobin synthesis, kidney, and lung problems [4–7]. In addition, the presence of Pb(II) in the human body causes bone problems by replacing it with calcium [8]. Given these problems, the US Environmental Protection Agency and the World Health Organization have determined acceptable concentrations of Pb(II) in drinking water at 0.015 and 0.01 mg/L, respectively [1]. Various

* Corresponding author.

methods have been used today to remove heavy metals from aqueous solutions, including precipitation, membrane filter, ion exchange, coagulation and flocculation, electrochemical, and adsorption [9–11]. Among these methods, the adsorption process due to features such as low cost, simplicity of design, insensitivity to toxic substances, and high availability has attracted further studies for the removal of metal contaminants [12–14]. In this method, the contaminants are transferred from the liquid phase to the solid phase, and thereby the biological access of toxic species to living organisms is reduced [15]. In the adsorption process, various adsorbents such as zeolite, chitosan, carbon nanotube, and activated carbon have been used to adsorb metals. However, these conventional adsorbents typically showed low adsorption capacity, hard separation, and high cost in practical applications [12,16].

Compared to the sorbent mentioned above, montmorillonite as a mineral clay has features such as high specific surface area, high cation exchange capacity, hydrophilicity, abundance, and low cost [17]. In addition, the magnetic montmorillonite (MMT) layer structure consists of central $AlO_4(OH)_2$ octahedral sheets and two SiO_4 tetrahedral sheets, which are ideal for pollutant adsorption, energy storage, and supporting nanocatalysts. Based on their unique structure and adsorption characteristics, many studies have recently used MMT as an adsorbent and supporting material to enhance catalytic and photocatalytic activities [18,19]. However, this method has disadvantages in the treatment processes, such as the tendency to aggregation and hard separation [20]. To solve this problem, considerable attention has recently been focused on the magnetization of the adsorbents [21]. This modification increases the mechanical strength, stability against the chemical compounds, and improvement of the surface area of the adsorbent [22]. This strategy has recently been used to modify sorbents, improve their removal efficiency, and recycle. Hashemian et al. [23] investigated the performance of bentonite/Fe_3O_4 nanocomposite for cobalt removal and found that Fe_3O_4 (98.44 m^2/g), in addition to increasing the specific surface area of nanocomposite (140.5 m^2/g), resulted in improving adsorption efficiency to 18.76 mg/g at alkaline pH. Van Lam et al. [24] used bentonite/Fe_3O_4 nanocomposite to remove lead and cadmium. Their results showed that the nanocomposite, by fitting with Freundlich isotherm, has superior efficiency compared to other materials. The above considerations showed the potential of the magnetic adsorbent in the removal of metals. However, little study has been performed on the treatment of solutions through the adsorption column.

The aim of the present study was to synthesize MMT/Fe_3O_4 nanoparticles by co-precipitation and its use as a Pb(II) adsorbent from aqueous solutions. The influence of pH, initial Pb(II) concentration, adsorbent dose, temperature, and stirring rate on adsorption efficiency was evaluated. Kinetic and isotherm studies were performed to investigate the adsorption rate. The mechanism of Pb(II) interaction with MMT/Fe_3O_4 was studied by Fourier-transform infrared spectroscopy (FTIR) and scanning electron microscopy (SEM)-mapping techniques. In order to check the adsorbent stability, the removal experiments were repeated with the same adsorbent. Finally, for evaluation of the feasibility of the Pb(II) adsorption process in practical applications, the packed adsorbent column with MMT/Fe_3O_4 was used.

2. Experimental section

2.1. Materials and reagents

All chemicals, including sulfuric acid (H_2SO_4, 95%), sodium hydroxide (NaOH, ≥97.0%), and ferric nitrate ($Fe(NO_3)_3{\cdot}9H_2O$, ≥99.999%) were purchased from Merck Co., (Germany) and were of analytical grade. The stock solution of Pb(II) was prepared at a suitable concentration by dissolving lead nitrate ($Pb(NO_3)_2$, ≥99%) in distilled water. Montmorillonite, with a particle size of 1–2 nm and a specific surface area of 220–270 m^2/g, was provided by an Iranian Nanomaterials Company (Mashhad, Iran).

2.2. Synthesis and characteristics of MMT/Fe_3O_4

MMT/Fe_3O_4 nanoparticles were synthesized by co-precipitation. First, 2 g $Fe(NO_3)_3{\cdot}9H_2O$ was dispersed in 100 mL distilled water and stirred at a constant speed for 30 min. Then 4 g of MMT was added to the mixture and stirring continued for another 30 min. The pH of the mixture was adjusted to 10–11 by adding 1 M NaOH. The mixture was stirred at 100°C for 60 min, and finally, the MMT/Fe_3O_4 product was separated by filtration and washed with distilled water several times and finally dried at 70°C for 12 h.

The morphology of synthesized adsorbent was characterized by field emission scanning electron microscopy (MIRA III Model, TESCAN, Czech) and transmission electron microscopy (TEM, JEOL-2010, Japan). The crystalline phase of MMT/Fe_3O_4 was detected by an X-ray diffractometer (XRD, PW 1730 Model, Philips) operated at 30 mA and 40 kV with Cu/Kα radiation with a range of 2θ from 10° to 80°. A thermogravimetric analysis (TGA) Q600 from TA Instruments (USA) was used to investigate the thermal stability properties of the synthesized adsorbent. The functional groups of the nanoparticles were determined by Fourier-transform infrared spectrometer at 400–4,000 cm^{-1}.

2.3. Batch and column adsorption experiments

All adsorption experiments were performed in 100 mL Erlenmeyer flasks. Aqueous solutions containing different concentrations of Pb (30–200 mg/L) were exposed to 0.05 g/L of MMT/Fe_3O_4 nanoparticles at different pH values (2–6) that were regulated by H_2SO_4 or NaOH at the start of the experiments. After mixing the solutions at different agitation speeds (100–300 rpm), the solution phase was separated from the adsorbent by centrifugation at different contact times (5–180 min), and the metal concentration was determined by an atomic absorption spectrophotometer (Younglin, 8020 AAS). In this study, all experiments were repeated three times. During the experiments, a control sample was used to ensure that Pb(II) concentration was not reduced in the solution without magnetic nanoparticles.

After optimizing the conditions by batch experiments, column experiments were performed using a plastic column (diameter of 5 cm and length of 20 cm) packed with magnetic nanoparticles (Fig. 1). In this method, the solution

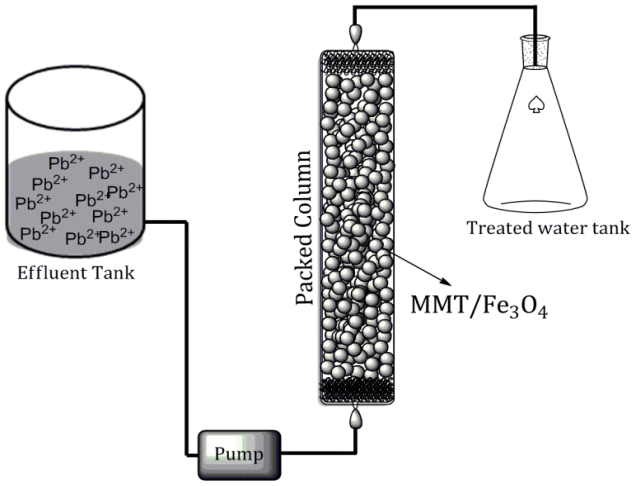

Fig. 1. Up-flow column for continuous testing.

containing Pb (30 mg/L) was passed through the column using a pump at a constant flow rate, and its outlet was measured to determine the amount of Pb removed. Adsorption isotherm experiments were performed at different concentrations (30–200 mg/L) at room temperature. The kinetic experiments were investigated for the Pb solution at contact times from 5 to 180 min. In all experiments, the amount of Pb adsorbed onto MMT/Fe_3O_4 (q_e, mg/g) and efficiency (R, %) were calculated by Eqs. (1) and (2), respectively.

$$q_e = \frac{(C_0 - C_t)V}{m} \tag{1}$$

$$R = \frac{(C_0 - C_t)}{C_0} \times 100 \tag{2}$$

where C_0 and C_t (mg/L) are the initial concentration and the concentration at time t, V (L) is the initial volume of solution and m (g) is the adsorbent weight.

To determine the point of zero charge of MMT/Fe_3O_4, 0.10 g of adsorbent was added to 25 mL of 0.01 M NaCl, and the initial pH of the solution (pH_i) in the range of 2–12 was then adjusted with 0.1 M HCl and NaOH. The mixture was mixed on a shaker for 24 h and the final pH (pH_f) of each sample was measured with a pH meter. The plot of the difference between pH_{f-i} vs. pH_i was plotted and pHpzc was obtained as an intercept on an x-axis.

2.4. Reusability of adsorbent

For practical applications, long-term use of the adsorbent for the treatment of aqueous solutions is essential. Hence, in the present study, to obtain the reusability of MMT/Fe_3O_4, the adsorption–desorption cycle was repeated five times using the same adsorbent. During the cycle, the adsorbent was separated by the filter and washed several times with distilled water, and reloaded in the reaction solution. Desorption of Pb(II) was performed using 50 mL of 0.1 M HNO_3 under room temperature. In this method, 0.1 g/L MMT/Fe_3O_4 containing the contaminant was placed in the desorption medium and stirred at a stirring rate of 300 rpm for 60 min. The suspension was then filtered, and the adsorbent was collected for the next cycle.

3. Results and discussion

3.1. Characteristics of MMT/Fe_3O_4

Figs. 2a–c show the SEM image of MMT, Fe_3O_4, and MMT/Fe_3O_4 nanoparticles. According to this figure, MMT and Fe_3O_4 were a large sheet and a spherical shape, respectively, while the synthesized MMT/Fe_3O_4 nanoparticles have a thick surface containing polygon particles. This indicates that the magnetic nanoparticles are coated on MMT. Analysis of the TEM image (Fig. 2d) confirms the SEM results and shows that high-density Fe_3O_4 is scattered over the surface of MMT. Fig. 2e shows the magnetic properties of the synthesized nanoparticles. The TGA analysis shown in Fig. 2f confirms the thermal stability of the nanoparticles in the temperature range of 0°C–1,000°C. In addition, the low reduction of MMT/Fe_3O_4 weight in this temperature range could be related to the evaporation of bonded water, desorption of crystal water, and loss of low amounts of hydroxyl structural groups.

The XRD pattern of MMT/Fe_3O_4 is shown in Fig. 3. According to the results of other studies [25], the characteristic peaks of the magnetic nanoparticles exist in the dispersed pattern of the synthesized nanoparticles, and the peaks revealed at 30.46°, 35.80°, and 54.06° are related to the hexagonal structure of MMT.

3.2. Performance of MMT/Fe_3O_4 compared to other adsorbents

To better understand the removal efficiency by MMT/Fe_3O_4, a comparison between Fe_3O_4 and MMT and their composite for removal of Pb(II) was conducted at a pH of 5 and adsorbent dosage of 0.025 g/L, and results were shown in Fig. 4. As can be seen, the removal efficiency of Pb(II) by MMT and Fe_3O_4 at a contact time of 90 min was 65% and 58%, respectively. These results indicate that both adsorbents have a remarkable ability to remove Pb(II) from aqueous solutions. In contrast, the efficiency of MMT/Fe_3O_4 for Pb(II) removal was 86%. This high efficiency may be due to the synergistic effect of MMT and Fe_3O_4 on the adsorption process and the increase of the adsorbent contact surface. Similar results were observed by Ge et al. [26] for the adsorption of methylene blue by magadiite–magnetite nanocomposite.

3.3. Effect of factors

To investigate the role of solution pH on the removal of Pb(II) by MMT/Fe_3O_4, adsorption experiments were carried out under pH values from 2 to 6. The pH values above 7 were not studied due to the precipitation of Pb(II) in the form of $Pb(OH)_2$. The results of Fig. 5a show that by increasing the pH from 2 to 5, the removal efficiency and the adsorption capacity of Pb(II) are increased at a high rate. In contrast, at pH above 5, the efficiency remains almost constant. These changes in efficiency can be explained by changes in the adsorbent and pollutant surface charge. PZC of MMT/Fe_3O_4

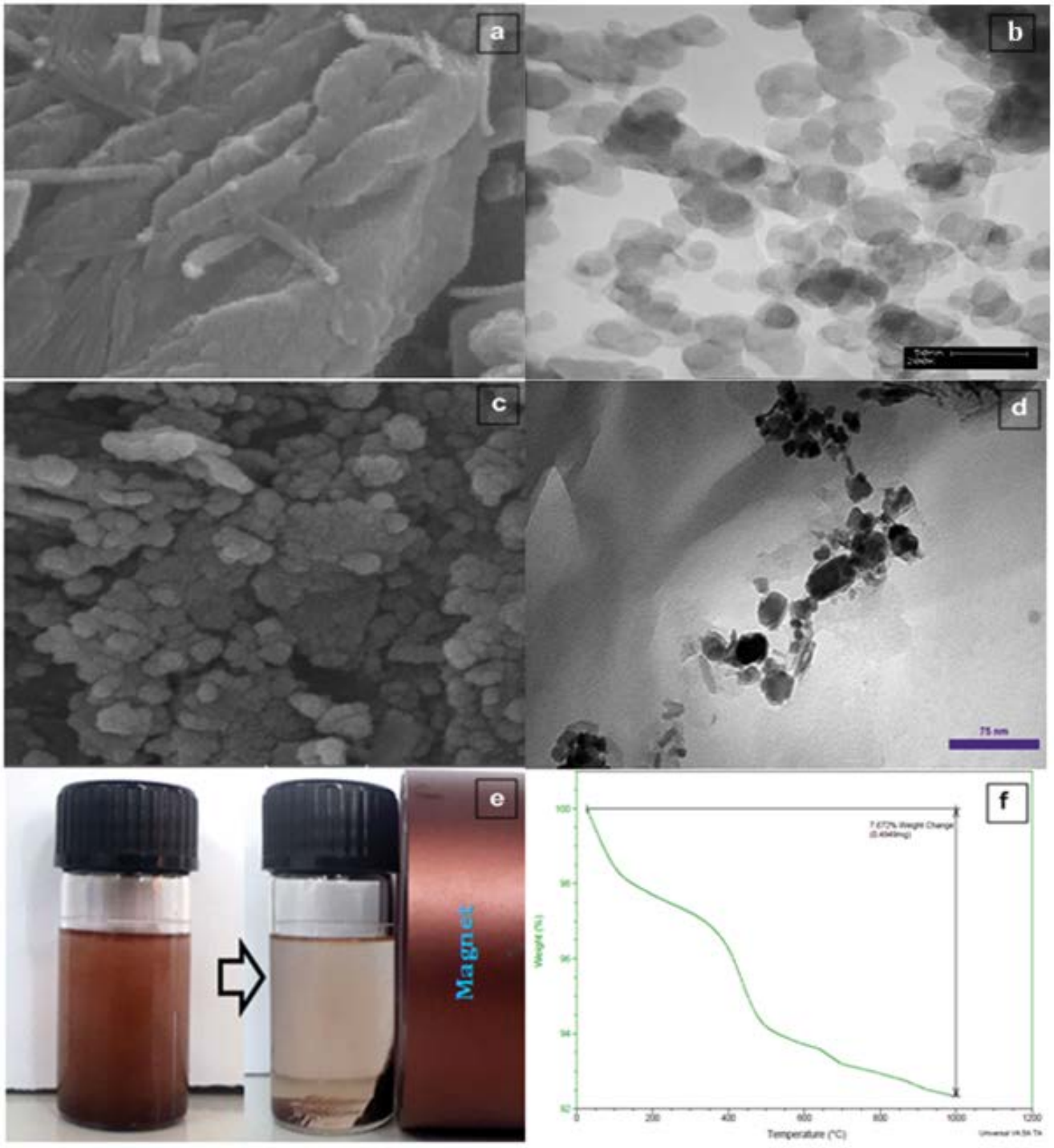

Fig. 2. SEM images of MMT (a), Fe_3O_4 (b) and MMT/Fe_3O_4 (c); TEM image (d), magnetic properties (e) and TGA curve of MMT/Fe_3O_4 (f).

nanoparticle was obtained 3.2 (Fig. 3b). The below this pH, the adsorbent surface is positive, while with increasing pH, the adsorbent surface will be negative. Based on this, at lower pH, a high amount of hydrogen ion (H^+) inhibits the adsorption of Pb(II), but with increasing pH, the electrostatic adsorption between the adsorbent and the contaminant is improved. Zhu et al. [27] reported similar results for Pb(II) adsorption by modified MMT/carbon composite. Fig. 5b shows the effect of MMT/Fe_3O_4 dosage on Pb(II) removal efficiency. According to this figure, the removal efficiency was improved from 90% to 98% by increasing the adsorbent dosage from 0.05 to 0.4 g/L. This could be due to the

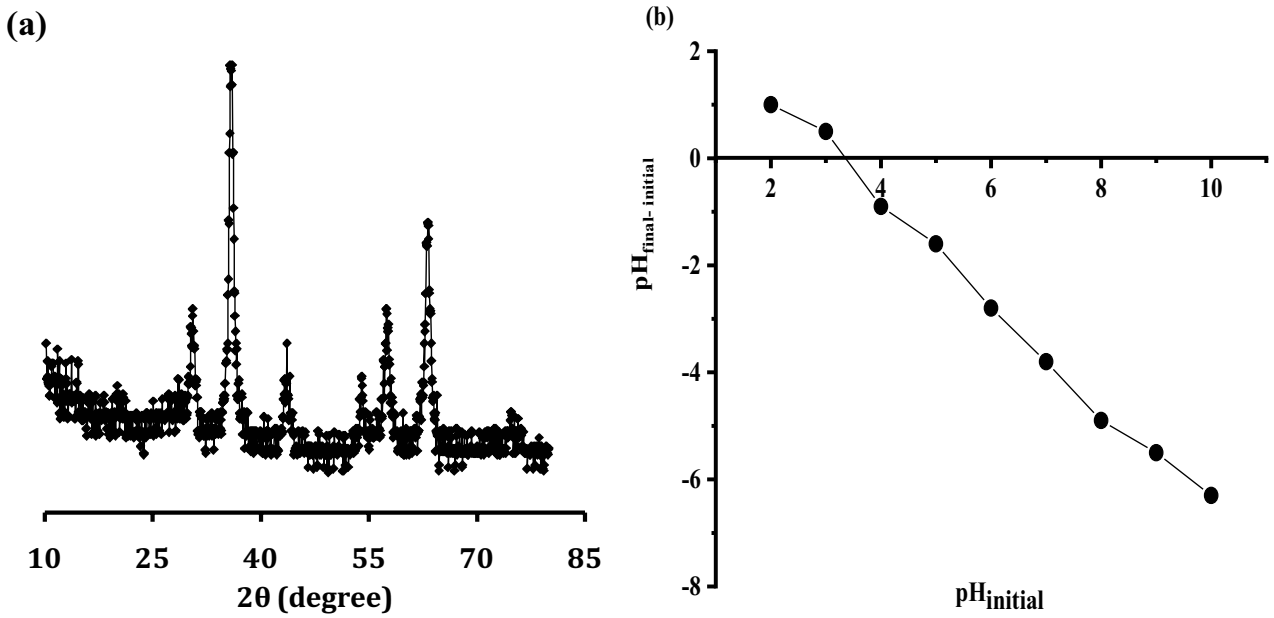

Fig. 3. XRD pattern (a) and point zero charge (b) of MMT/Fe_3O_4.

increase in the number of active sites of the adsorbent for Pb(II) adsorption. This figure also showed that the adsorption capacity decreased from 54 to 7.34 mg/g as the adsorbent dosage increased from 0.05 to 0.4 g/L. Similar results were found by Shen et al. [28] for the adsorption of Pb(II) by MMMT@Zn-BDC from aqueous solutions.

The effect of the initial Pb(II) concentration of 30–200 mg/L on its removal efficiency was investigated at a contact time of 90 min, and its results are shown in Fig. 5c. As can be seen, increasing the initial Pb(II) concentration from 30 to 200 mg/L reduced the removal efficiency from 96% to 43%. This may be due to the saturation of the adsorption sites on the adsorbent. However, the actual amount of Pb(II) adsorbed on MMT/Fe_3O_4 increases. This can be attributed to the high driving force for mass transfer at high concentrations of contaminant. Farghali et al. [29] observed similar results for Pb(II) adsorption by CuO nanoparticles. Fig. 5d shows the effect of contact time on the removal efficiency of Pb(II) at pH of 5, adsorbent dose of 0.4 g/L, and initial Pb(II) concentration of 30 mg/L. According to this figure, by increasing the initial contact time from 5 to 120 min, the removal efficiency and the Pb(II) adsorption capacity are increased. This may be due to the fact that all MMT/Fe_3O_4 adsorption sites were initially empty, and the concentrations of contaminants are high. However, with a further increase in contact time (>120 min), the removal efficiency decreased due to the decrease in the adsorption active sites. The study of the influence of stirring rate on the adsorption of Pb(II) is shown in Fig. 5e. This can be observed that by increasing the stirring rate, the adsorption efficiency increases. This could be due to the increase in the adsorbent and adsorbate collisions as well as the decrease of the boundary layer thickness around MMT/Fe_3O_4. Similar results were observed by Hanafiah et al. [30] for adsorption of acid blue 25. Fig. 5f shows the influence of temperature in the removal efficiency and adsorption capacity of Pb(II) by

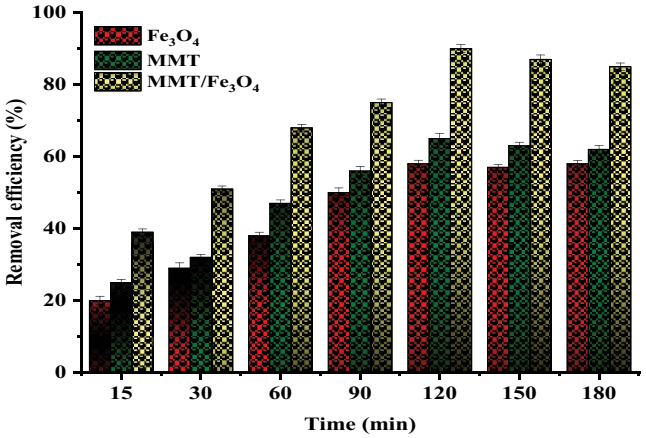

Fig. 4. Removal of Pb(II) by various adsorbents.

MMT/Fe_3O_4 at pH of 5, adsorbent dose of 0.075 g/L, and reaction time of 90 min. According to this figure, as the temperature increases from 25°C to 45°C, the removal rate increases from 90% to 98.9%, while the Pb(II) adsorption capacity is increased from 36 to 39.56 mg/g. Qu et al. [31] reported similar results for the influence of temperature on Pb(II) adsorption.

3.4. Kinetics studies

To evaluate the mass transfer rate in the adsorption process, the pseudo-first-order and pseudo-second-order kinetic models are used repeatedly [32]. Eqs. (3)–(4) show the linear form of these kinetics. In these equations, q_e and q_t are the adsorption capacity in equilibrium and at time t (mg/g), respectively. k_1 and k_2 represent the rate constants of first and second-order kinetic models (min^{-1}), respectively.

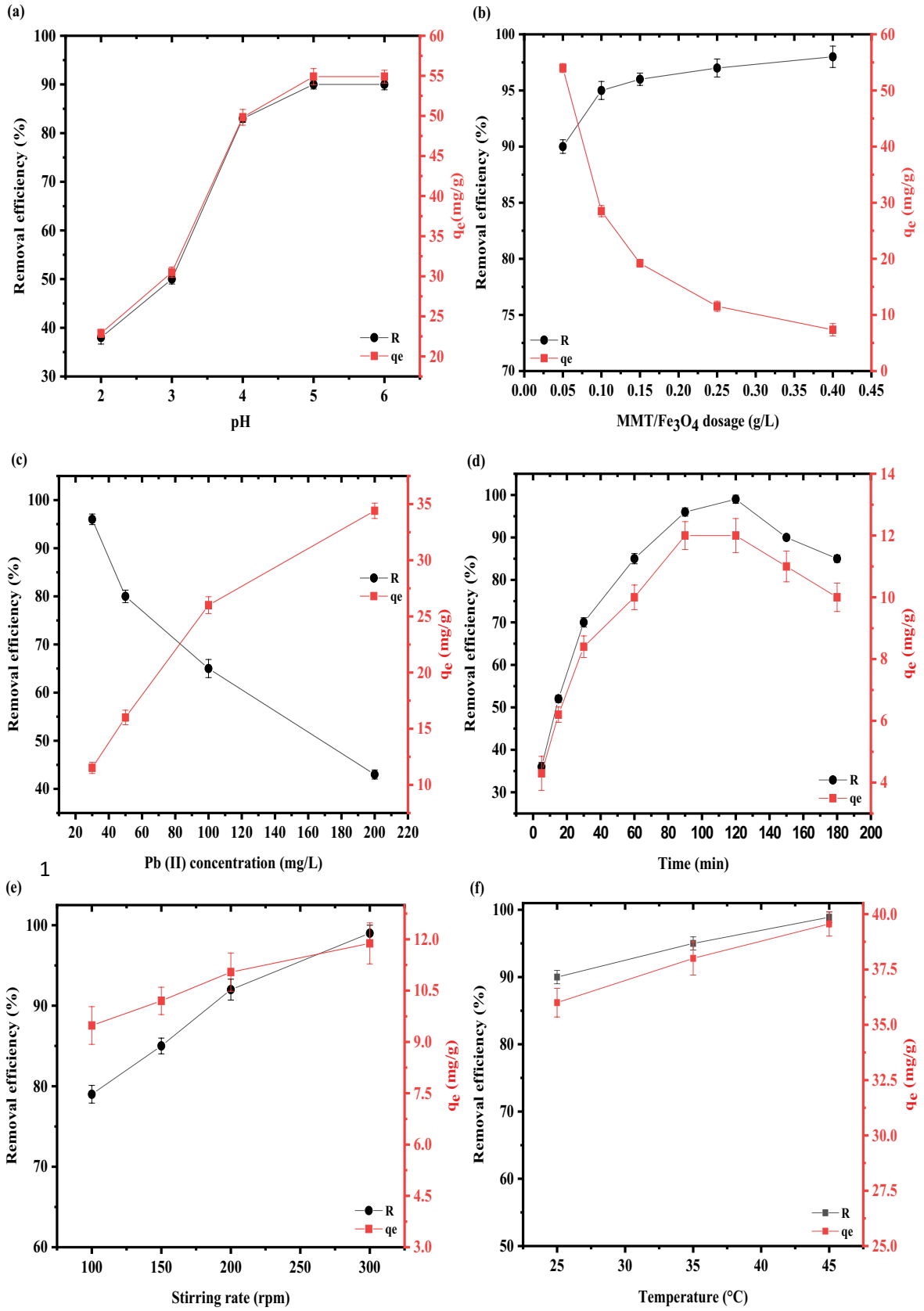

Fig. 5. Effect of pH (a), MMT/Fe_3O_4 dosage (b), Pb(II) concentration (c), contact time (d), stirring rate (e) and temperature (f) on removal efficiency and adsorption capacity of Pb(II).

The calculated parameters for the kinetic models and fitted experimental data are shown in Table 1. As can be seen, the correlation coefficient (R^2) of the pseudo-second-order model was higher than that of the pseudo-first-order model. In addition, the amount of q_e calculated by the second-order kinetic model is in good agreement with the experimental q_e, which indicates that chemisorption is the predominant mechanism of Pb(II) adsorption on MMT/Fe_3O_4.

In order to further investigate the kinetics of adsorption and to further confirm the chemisorption characteristic, the Elovich kinetic model was studied according to Eq. (5). In this equation, α is the initial adsorption rate and 1/ß represents the sites accessible for chemisorption. The results in Table 1 show R^2 values > 0.98 for fitting the experimental data by the Elovich model and the higher values of 1/ß explained the numerous available sites on MMT/Fe_3O_4 for chemisorption.

In addition to the above kinetics, in most studies further analysis is performed using the intraparticle diffusion equation to study the diffusion rate-limiting [33]. By plotting q_t against $t^{0.5}$ of Eq. (6), the constant of reaction rate of the intraparticle diffusion model (k_{id}) can be achieved from the slope (mg/g $min^{1/2}$), and the boundary layer thickness (C) can be obtained from the intercept. Considering Table 1, it can be seen that the curve is almost a straight line with an R^2 value equal to 0.98, but the line did not pass through the origin because the constant value of C was different from zero and was 2.411. This means that pore diffusion was not the only controlling step. Similar results were reported by Berrazoum et al. [33].

$$\ln\left(q_e - q_t\right) = \ln q_e - k_1 t \tag{3}$$

$$\frac{t}{q_t} = \frac{1}{k_2 q_e^2} + \frac{t}{q_e} \tag{4}$$

$$q_t = \frac{1}{\beta}\ln\left(\alpha\beta\right) + \frac{1}{\beta}\ln\left(t\right) \tag{5}$$

$$q_t = k_{id} t^{0.5} + C \tag{6}$$

3.5. Adsorption isotherm

The parameters obtained from different adsorption isotherm models can provide good information on the adsorption behavior and adsorbent surface properties. In addition, analyzing isotherm data by fitting it to different models is one of the key steps in finding an isotherm model that can be used for adsorption process design purposes. Therefore, the adsorption isotherm study was performed by six models of Langmuir, Freundlich, Temkin, Dubinin–Radushkevich, Elovich, and Harkins–Jura isotherm. The Langmuir isotherm is used for monolayer adsorption systems and is valid for layer adsorption onto a large number of sites, while the Freundlich equation is an empirical equation to explain the heterogeneous system. The Dubinin–Radushkevich isotherm is used to estimate the characteristic porosity and free energy of adsorption. The Temkin isotherm model considers the interaction of the indirect adsorbate/adsorbate in the adsorption process. The Harkins–Jura isotherm model assumes the possibility of multilayer adsorption on the surface of the adsorbents with heterogeneous pore distribution. The linear equations of the isotherms used are as follows:

Langmuir isotherm:

$$\frac{C_e}{q_e} = \frac{1}{bq_m} + \frac{C_e}{q_m} \tag{7}$$

Freundlich isotherm:

$$\log q_e = \log k_f + \frac{1}{n}\log C_e \tag{8}$$

Temkin:

$$q_e = B\ln K_T + B\ln C_e \tag{9}$$

Dubinin–Radushkevich:

$$\ln q_e = \ln q_m - \beta\left(RT\ln\left(1+\frac{1}{C_e}\right)\right)^2 \tag{10}$$

Elovich:

$$\ln\frac{q_e}{C_e} = \ln K_F q_m - \frac{q_e}{q_m} \tag{11}$$

Table 1
Kinetic parameters for the adsorption of Pb(II) by MMT/Fe_3O_4

	First-order kinetic model			Second-order kinetic model		
$q_{e,exp}$ (mg/g)	k_1 (min^{-1})	$q_{e,cal}$ (mg/g)	R^2	k_2 (g/mg min)	$q_{e,cal}$ (mg/g)	R^2
11.88	0.034	189.93	0.975	0.021	13.03	0.992
	Intraparticle diffusion			Elovich kinetic model		
	K_p (g/mg $min^{0.5}$)	C	R^2	α (mg/g min)	1/ß (mg/g)	R^2
	0.993	2.411	0.985	2.44	2.51	0.986

Harkins–Jura:

$$\frac{1}{q_e^2}=\left(\frac{B_{HJ}}{A_{HJ}}\right)-\left(\frac{1}{A_{HJ}}\right)\log C_e \quad (12)$$

where q_e is the adsorbed Pb(II) amount per gram of adsorbent (mg/g), C_e is the equilibrium concentration of Pb(II) in solution (mg/L), q_m is the maximum adsorption capacity of the adsorbent (mg/g), K_F, n, and b are the equilibrium constants, K_T is Temkin isotherm equilibrium binding constant (L/g), B is constant related to the heat of sorption (J/mol), R is the gas constant (8.314 J/mol K), T is the absolute temperature (K), β is the constant of the sorption energy (mol²/J²), K_E is the Elovich equilibrium constant (L/mg), A_{HJ} is Harkins–Jura isotherm parameter which accounts for multilayer adsorption and explains the existence of heterogeneous pore distribution, while H_{JB} is the isotherm constants, respectively.

The regression value (R^2) shown in Table 2, explains that the adsorption data fit well with the Langmuir isotherm. The appropriate fit of the experimental data to the Langmuir isotherm showed a physical sorption mechanism. Table 2 also showed that the maximum adsorption of MMT/Fe_3O_4 for Pb(II) could occur up to 36.76 mg/g.

The magnitude of the coefficient n indicates the desirability of the adsorption, and it is stated that its values in the range 2–10 indicate good adsorption; the values between 1 and 2 reveal relatively difficult adsorption, and the values less than 1 is the characteristic of poor adsorption. According to the results of Table 2, MMT/Fe_3O_4 nanoparticles are a suitable adsorbent for Pb(II). Besides, it has been reported that the adsorption process can be considered as physical adsorption when the amount of free energy (E) is less than 8 kJ/mol. Conversely, if the amount of free energy is between 8 and 16 kJ/mol, the type of adsorption can be explained by ion exchange and for the values higher than 16 kJ/mol, and the type of adsorption can be expressed based on chemical adsorption. Based on the E values calculated from Eq. (13) it can be found that the type of Pb(II) adsorption on MMT/Fe_3O_4 is physical.

$$E=\frac{1}{\sqrt{2\beta}} \quad (13)$$

The optimum nature of adsorption can also be calculated according to the equation $R_L = 1/(1 + bC_0)$, where R_L is dimensionless separation factors, b is Langmuir constant, and C_0 is the initial concentration of Pb(II) in solution. The values of R_L indicate that the isotherm type is irreversible ($R_L = 0$), favorable ($0 < R_L < 1$), linear ($R_L = 1$) or unfavorable ($R_L > 1$). According to Table 2, the mean separation factor calculated for Pb(II) on MMT/Fe_3O_4 was 0.04–0.23, which indicates favorable adsorption. The B value of 5.05 J/mol also explained that the bond between the adsorbent and the adsorbate is suitable. In addition to the above results, the adsorption data fitted with the Harkins–Jura model confirm the occurrence of multilayer adsorption due to the heterogeneous pore distribution. The maximum adsorption capacity determined by the linear Elovich equation (Table 2) is close to the values obtained by experimental adsorption, which means that the multilayer adsorption occurs on the adsorbent in the range of concentrations studied.

Table 3 shows a comparison of the maximum adsorption capacity of Pb(II) on different adsorbents. As can be seen, the capacity of adsorbents to adsorb contaminants is very variable, which may be due to the different characteristics of the adsorbent provided, the operating conditions, and the type of contaminants. However, MMT/Fe_3O_4 has a higher adsorption capacity for Pb(II) compared to other reported adsorbents. These results suggest that MMT/Fe_3O_4 adsorbent can be considered as an adsorbent of Pb(II) from aqueous solutions.

3.6. Adsorbent stability and adsorption mechanism

The FTIR spectra of MMT/Fe_3O_4 nanoparticles before and after the adsorption process are shown in Fig. 6a. As can be seen in the FTIR before adsorption, the band around 1,000 cm^{-1} is related to Al–Al–OH, and the band in the range 3,400–3,600 cm^{-1} is related to the stretching vibration of the structural OH group of MMT. The band stretched at 550–570 cm^{-1} can be related to Fe–O stretching vibration. Previous studies have also linked this range of FTIR to Si–O and Al–OH [40]. After the adsorption process, the peaks were significantly altered around 500–600 cm^{-1} and 1,000 cm^{-1}, which could be due to the activity of the Al–OH and Fe–O functional groups in the adsorption of Pb(II). To confirm the adsorption

Table 2
Isotherm parameters for Pb(II) adsorption by MMT/Fe_3O_4

Freundlich isotherm			Langmuir isotherm			
n	K_F (mg/g)	R^2	b	q_{max} (mg/g)	R^2	R_L (L/mg)
4.06	10.36	0.966	0.106	36.76	0.989	0.04–0.23
Temkin isotherm			Dubinin–Radushkevich isotherm			
K_T (L/mg)	B (J/mol)	R^2	β (mol²/J²)	E (kJ/mol)	R^2	
5.24	5.05	0.919	4×10^{-7}	0.354	0.602	
Elovich isotherm			Harkins–Jura isotherm			
q_e (mg/g)	K_E (L/mg)	R^2	A_{HJ}	B_{HJ}	R^2	
7.418	1.55	0.885	258.71	2.171	0.9719	

Table 3
Comparison of MMT/Fe_3O_4 efficiency with other adsorbents in Pb(II) adsorption

Adsorbent	Isotherm	Kinetic model	q_e (mg/g)	Reference
Carbon nanotubes	Langmuir	Pseudo-second-order	11.23	[34]
Nanometer titanium dioxide immobilized on silica gel	–	–	3.16	[35]
Seed husk of *Calophyllum inophyllum*	Langmuir	Pseudo-second-order	34.51	[36]
Chitosan beads	Freundlich	–	34.98	[37]
Chitosan – GLA beads	Freundlich	–	14.24	[37]
Bacterial cellulose	Langmuir	Pseudo-second-order	24.59	[38]
Peat	Redlich–Peterson	Pseudo-second-order	15	[39]
MMT/Fe_3O_4	Langmuir	Pseudo-second-order	36.76	Present study

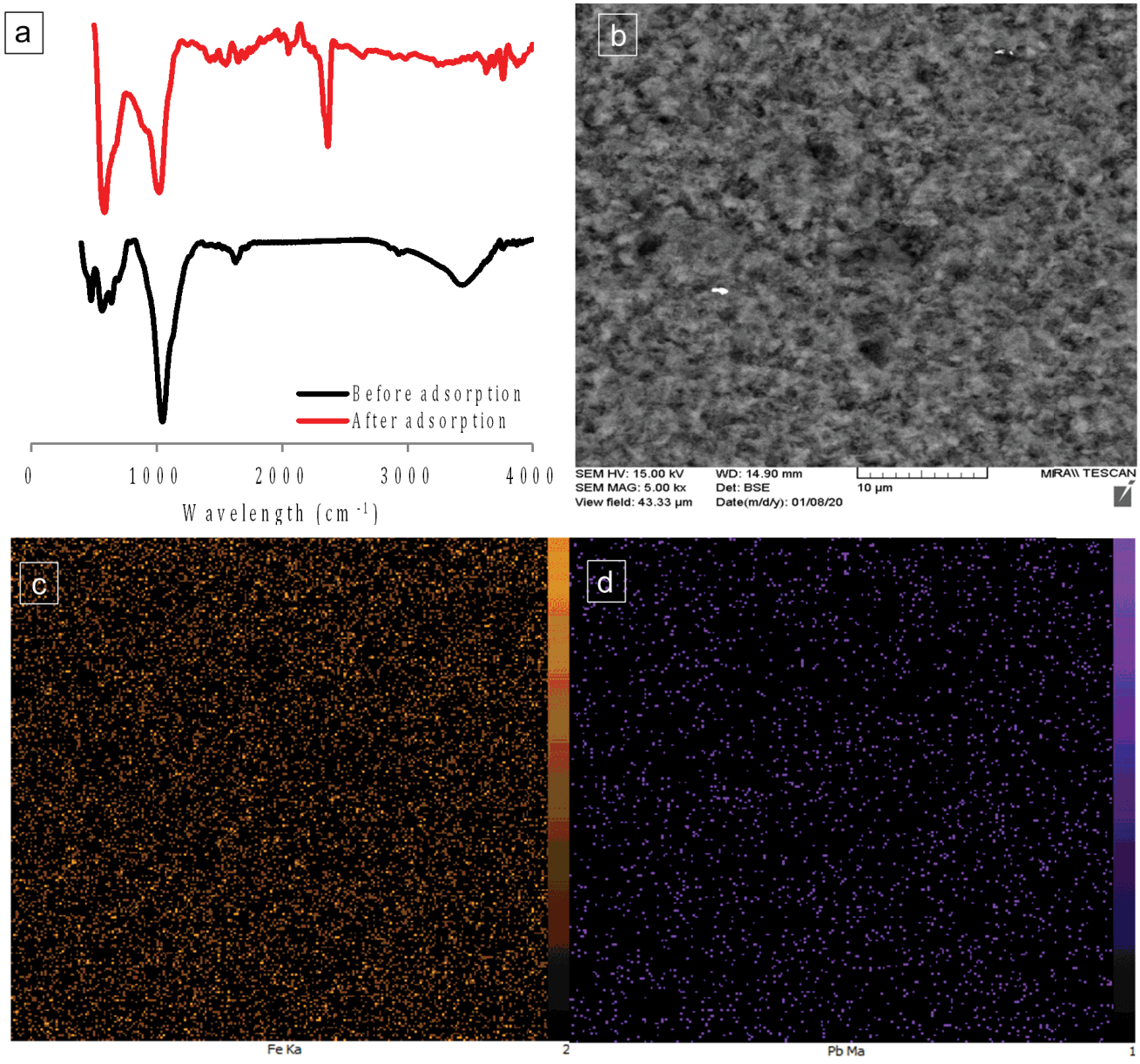

Fig. 6. FTIR spectra of MMT/Fe_3O_4 before and after adsorption of Pb(II); SEM-mapping of MMT/Fe_3O_4 after adsorption of Pb(II).

of Pb(II) metal on the adsorbent, SEM-mapping experiments were performed, and the results in Figs. 6b–d showed that the metal contaminant was uniformly adsorbed on the MMT/Fe_3O_4 surface.

The stability and recyclability of MMT/Fe_3O_4 adsorbents were investigated using adsorption–desorption experiments and the results in Fig. 7a showed that the removal efficiency and the adsorption capacity of the pollutant decreased after 4 consecutive cycles. This could be due to the occupation of the adsorption sites and their destruction during the adsorption–desorption process. Similar results were observed by Samuel et al. [1] for the uptake of Pb(II).

For the feasibility study of MMT/Fe_3O_4 activity in real applications, the adsorbent column was used to treat the real sample, and the results were shown in Fig. 7b. Accordingly, the efficiency of the adsorbent column is lower than that of the batch experiments, which may be due to the particle aggregation and subsequent reduction of the specific surface area. The results of Fig. 7b also showed that the treatment efficiency of the real sample was lower than that of the synthetic sample, which could be related to the high content of organic matter and occupation of the adsorbent surface by them. Considering the above considerations, MMT/Fe_3O_4 with suitable surface area, its reusability, and high stability can be used as a suitable adsorbent. Based on the isotherm and kinetic documents and FTIR results, we propose a Pb(II) adsorption mechanism by MMT/Fe_3O_4 (Fig. 8). When the adsorbent is added to the water containing Pb(II), the Pb(II) ion is adsorbed on the MMT/Fe_3O_4 surface by chemical or electrostatic adsorption. In addition, the presence of MMT as a supporting material increases the adsorption band for Pb(II).

4. Conclusion

In summary, MMT/Fe_3O_4 nanoparticles were chemically synthesized and then used to adsorb Pb(II) from the aqueous solution. The results of comparative experiments showed that Fe_3O_4 coating on MMT significantly increased the Pb(II) adsorption capacity. The results also indicated that the removal of Pb(II) on the adsorbent depends on the initial pH, adsorbent dosage, initial Pb(II) concentration, temperature, and stirring rate. The adsorption data follows from

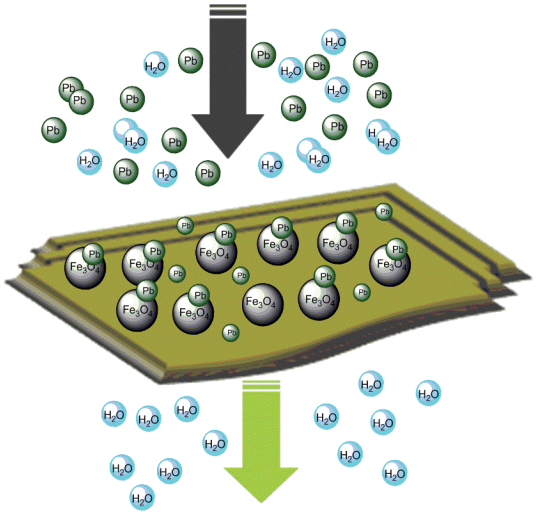

Fig. 8. Adsorption mechanism between the MMT/Fe_3O_4 and Pb(II).

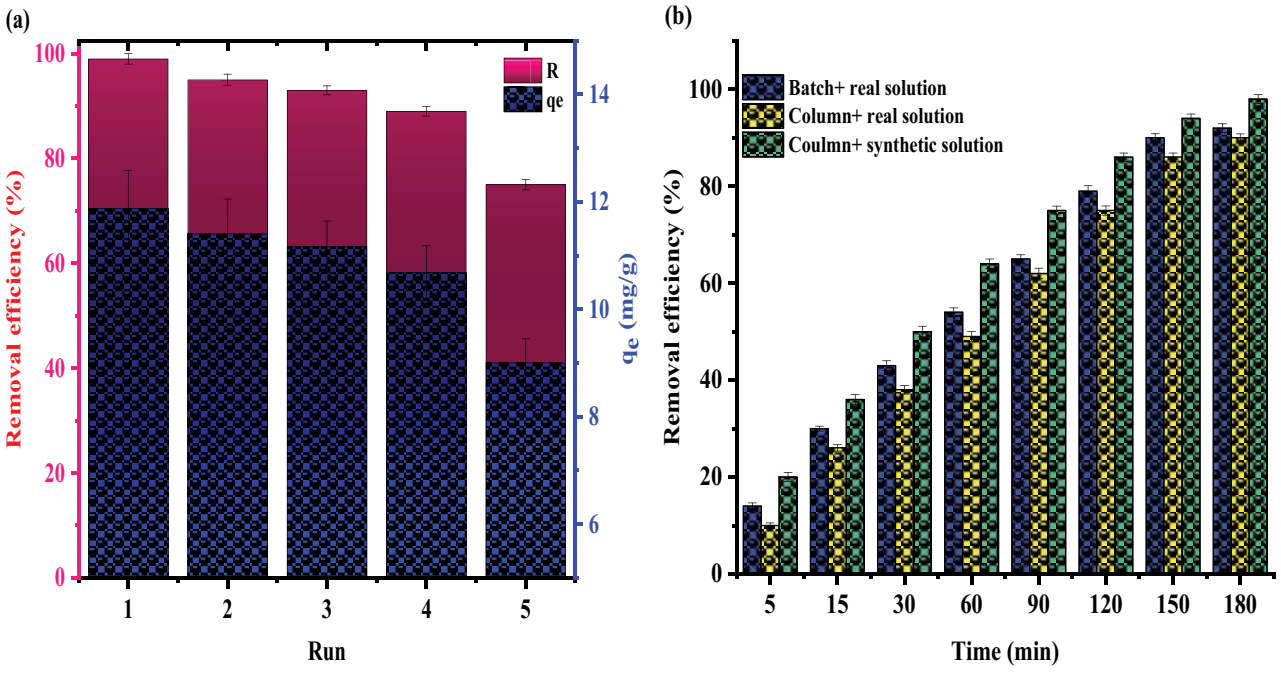

Fig. 7. Reusability of the MMT/Fe_3O_4 in cycle reaction of adsorption–desorption (a) and treatment of real solution by adsorption process in batch and continuous modes (b).

pseudo-second-order kinetics, and a contact time of 120 min is required to obtain equilibrium. The isotherm data are in good agreement with the Langmuir isotherm, and the maximum adsorption capacity by MMT/Fe_3O_4 can be 36.76 mg/g. The average amount of adsorption energy (E = 0.354 kJ/mol) obtained from the Dubinin–Radushkevich isotherm showed that the adsorption of Pb(II) on the adsorbent was physical. Column study data showed the appropriate efficacy of MMT/Fe_3O_4 in the treatment of real wastewater containing Pb(II). The Pb(II) adsorption mechanism on MMT/Fe_3O_4 based on FTIR analysis is proposed, and SEM-mapping analysis confirmed the appropriate adsorption of the Pb(II) on the adsorbent. Based on the results, it can be concluded that MMT/Fe_3O_4 can be effectively used to remove Pb(II) from aqueous solutions due to its features such as magnetic separation, recyclability, and high stability.

Acknowledgments

This work was supported by the Environmental Health Research Center of Golestan University of Medical Sciences (No. 951217300).

References

[1] M.S. Samuel, Sk.S. Shah, J. Bhattacharya, K. Subramaniam, N.D. Pradeep Singh, adsorption of Pb(II) from aqueous solution using a magnetic chitosan/graphene oxide composite and its toxicity studies, Int. J. Biol. Macromol., 115 (2018) 1142–1150.

[2] L.P. Lingamdinne, J.R. Koduru, Y.-Y. Chang, R.R. Karri, Process optimization and adsorption modeling of Pb(II) on nickel ferrite-reduced graphene oxide nano-composite, J. Mol. Liq., 250 (2018) 202–211.

[3] J.J. Qu, Y. Li, T. Song, S. Huang, Y.N. Wei, X.S. Liu, H.M. Wang, Y. Jin, Comparison of the adsorption characteristics and mechanism of Pb onto four adsorbents derived from edible fungi spent substrate, Ecol. Eng., 142 (2020) 105639, doi: 10.1016/j.ecoleng.2019.105639.

[4] N.A.H. Mohamad Zaidi, L.B.L. Lim, A. Usman, Enhancing adsorption of Pb(II) from aqueous solution by NaOH and EDTA modified *Artocarpus odoratissimus* leaves, J. Environ. Chem. Eng., 6 (2018) 7172–7184.

[5] X.Z. Bian, Y. Xia, T.T. Zhan, L. Wang, W. Zhou, Q.Z. Dai, J.M. Chen, Electrochemical removal of amoxicillin using a Cu doped PbO_2 electrode: electrode characterization, operational parameters optimization and degradation mechanism, Chemosphere, 233 (2019) 762–770.

[6] L.B.L. Lim, N. Priyantha, Y.C. Lu, N.A.H.M. Zaidi, Adsorption of heavy metal lead using *Citrus grandis* (Pomelo) leaves as low-cost adsorbent, Desal. Water Treat., 166 (2019) 44–52.

[7] N. Priyantha, L.B.L. Lim, N.H.M. Mansor, A.B. Liyandeniya, Irreversible sorption of Pb(II) from aqueous solution on breadfruit peel to mitigate environmental pollution problems, Water Sci. Technol., 80 (2019) 2241–2249.

[8] Q. Ul Ain, H.B. Zhang, M. Yaseen, U. Rasheed, K. Liu, S. Subhan, Z.F. Tong, Facile fabrication of hydroxyapatite-magnetite-bentonite composite for efficient adsorption of Pb(II), Cd(II), and crystal violet from aqueous solution, J. Cleaner Prod., 247 (2020) 119088, doi: 10.1016/j.jclepro.2019.119088.

[9] F.L. Fu, Q. Wang, Removal of heavy metal ions from wastewaters: a review, J. Environ. Manage., 92 (2011) 407–418.

[10] Z. Noorimotlagh, R. Darvishi Cheshmeh Soltani, Gh. Shams Khorramabadi, H. Godini, M. Almasian, Performance of wastewater sludge modified with zinc oxide nanoparticles in the removal of methylene blue from aqueous solutions, Desal. Water Treat., 57 (2016) 1692–1684.

[11] Z. Noorimotlagh, M. Ravanbakhsh, M.R. Valizadeh, B. Bayati, G.Z. Kyzas, M. Ahmadi, N. Rahbar, N. Jaafarzadeh, Optimization and genetic programming modeling of humic acid adsorption onto prepared activated carbon and modified by multi-wall carbon nanotubes, Polyhedron, 179 (2020) 114354, doi: 10.1016/j.poly.2020.114354.

[12] D. Wu, Y.G. Wang, Y. Li, Q. Wei, L.H. Hu, T. Yan, R. Feng, L.G. Yan, B. Du, Phosphorylated chitosan/$CoFe_2O_4$ composite for the efficient removal of Pb(II) and Cd(II) from aqueous solution: adsorption performance and mechanism studies, J. Mol. Liq., 277 (2019) 181–188.

[13] M. Rafatullah, O. Sulaiman, R. Hashim, A. Ahmad, Adsorption of methylene blue on low-cost adsorbents: a review, J. Hazard. Mater., 177 (2010) 70–80.

[14] N. Jaafarzadeh, Z. Baboli, Z. Noorimotlagh, S.S. Martínez, M. Ahmadi, S. Alavi, S.A. Mirzaee, Efficient adsorption of bisphenol A from aqueous solutions using low-cost activated carbons produced from natural and synthetic carbonaceous materials, Desal. Water Treat., 154 (2019) 177–187.

[15] M.C. Ribas, M.A. Adebayo, L.D.T. Prola, E.C. Lima, R. Cataluña, L.A. Feris, M.J. Puchana-Rosero, F.M. Machado, F.A. Pavan, T. Calvete, Comparison of a homemade cocoa shell activated carbon with commercial activated carbon for the removal of reactive violet 5 dye from aqueous solutions, Chem. Eng. J., 248 (2014) 315–326.

[16] G.X. Zhao, X.L. Wu, X.L. Tan, X.K. Wang, Sorption of heavy metal ions from aqueous solutions: a review, Open Colloid Sci. J., 4 (2011) 19–31.

[17] S. Zhu, M.Z. Xia, Y.T. Chu, M.A. Khan, W. Lei, F. Wang, T. Muhmood, A. Wang, Adsorption and desorption of Pb(II) on L-Lysine modified montmorillonite and the simulation of interlayer structure, Appl. Clay Sci., 169 (2019) 40–47.

[18] N. Wang, F.Y. Xiao, J.L. Zhang, H.S. Zhou, Y.W. Qin, D.W. Pan, Spherical montmorillonite-supported nano-silver as a self-sedimentary catalyst for methylene blue removal, Appl. Clay Sci., 174 (2019) 146–151.

[19] K. Peng, H.J. Wang, X.Y. Li, J.W. Wang, L. Xu, H.F. Gao, M. Niu, M.B. Ma, J. Yang, One-step hydrothermal growth of MoS_2 nanosheets/CdS nanoparticles heterostructures on montmorillonite for enhanced visible light photocatalytic activity, Appl. Clay Sci., 175 (2019) 86–93.

[20] Z.W. Gao, X.J. Peng, H.M. Zhang, Z.K. Luan, B. Fan, Montmorillonite–Cu(II)/Fe(III) oxides magnetic material for removal of cyanobacterial *Microcystis aeruginosa* and its regeneration, Desalination, 247 (2009) 337–345.

[21] A.A. Mohammed, I.S. Samaka, Bentonite coated with magnetite Fe_3O_4 nanoparticles as a novel adsorbent for copper(II) ions removal from water/wastewater, Environ. Technol. Innovation, 10 (2018) 162–174.

[22] Y.D. Shahamat, M.A. Zazouli, M.R. Zare, N. Mengelizadeh, Catalytic degradation of diclofenac from aqueous solutions using peroxymonosulfate activated by magnetic MWCNTs-$CoFe_3O_4$ nanoparticles, RSC Adv., 9 (2019) 16496–16508.

[23] S. Hashemian, H. Saffari, S. Ragabion, Adsorption of cobalt(II) from aqueous solutions by Fe_3O_4/bentonite nanocomposite, Water Air Soil Pollut., 226 (2015) 2212, doi: 10.1007/s11270-014-2212-6.

[24] P. Van Lam, N.B. Duong, Q.T.T. Trang, V.A. Tuan, Removal of Pb^{2+} and Cd^{2+} ions from aqueous solutions using Fe_3O_4/bentonite nanocomposite, Vietnam J. Chem., 56 (2018) 617–622.

[25] M. Sadeghi, M.H. Mehdinejad, N. Mengelizadeh, Y. Mahdavi, H. Pourzamani, Y. Hajizadeh, M.R. Zare, Degradation of diclofenac by heterogeneous electro-Fenton process using magnetic single-walled carbon nanotubes as a catalyst, J. Water Process Eng., 31 (2019) 100852, doi: 10.1016/j.jwpe.2019.100852.

[26] M.L. Ge, Z.Z. Xi, C.P. Zhu, G.D. Liang, G.Q. Hu, L. Jamal, S.M. Jahangir Alam, Preparation and characterization of magadiite–magnetite nanocomposite with its sorption performance analyses on removal of methylene blue from aqueous solutions, Polymers, 11 (2019) 607, doi: 10.3390/polym11040607.

[27] K.C. Zhu, H.Z. Jia, F. Wang, Y.Q. Zhu, C.Y. Wang, C.Y. Ma, Efficient removal of Pb(II) from aqueous solution by modified

montmorillonite/carbon composite: equilibrium, kinetics, and thermodynamics, J. Chem. Eng. Data, 62 (2017) 333–340.
[28] J. Shen, N. Wang, Y.G. Wang, D. Yu, X.-k. Ouyang, Efficient adsorption of Pb(II) from aqueous solutions by metal organic framework (Zn-BDC) coated magnetic montmorillonite, Polymers, 10 (2018) 1383, doi: 10.3390/polym10121383.
[29] A.A. Farghali, M. Bahgat, A. Enaiet Allah, M.H. Khedr, Adsorption of Pb(II) ions from aqueous solutions using copper oxide nanostructures, Beni-Suef Univ. J. Basic Appl. Sci., 2 (2013) 61–71.
[30] M.A.K.M. Hanafiah, W.S.W. Ngah, S.H. Zolkafly, L.C. Teong, Z.A.A. Majid, Acid Blue 25 adsorption on base treated *Shorea dasyphylla* sawdust: kinetic, isotherm, thermodynamic and spectroscopic analysis, J. Environ. Sci., 24 (2012) 261–268.
[31] J.H. Qu, X. Tian, Z. Jiang, B. Cao, M.S. Akindolie, Q. Hu, C.C. Feng, Y. Feng, X.L. Meng, Y. Zhang, Multi-component adsorption of Pb(II), Cd(II) and Ni(II) onto microwave-functionalized cellulose: kinetics, isotherms, thermodynamics, mechanisms and application for electroplating wastewater purification, J. Hazard. Mater., 387 (2020) 121718, doi: 10.1016/j.jhazmat.2019.121718.
[32] M.H. Mehdinejad, N. Mengelizadeh, A. Bay, H. Pourzamani, Y. Hajizadeh, N. Niknam, A.H. Moradi, M. Hashemi, H. Mohammadi, Adsorption of methylene blue from aqueous solutions by cellulose and nanofiber cellulose and its electrochemical regeneration, Desal. Water Treat., 110 (2018) 250–263.
[33] A. Berrazoum, R. Marouf, F. Ouadjenia, J. Schott, Bioadsorption of a reactive dye from aqueous solution by municipal solid waste, Biotechnol. Rep. (Amst), 7 (2015) 44–50.
[34] S.-H. Hsieh, J.-J. Horng, Adsorption behavior of heavy metal ions by carbon nanotubes grown on microsized Al_2O_3 particles, J. Univ. Sci. Technol. Beijing Mineral Metall. Mater., 14 (2007) 77–84.
[35] R. Liu, P. Liang, Determination of trace lead in water samples by graphite furnace atomic absorption spectrometry after preconcentration with nanometer titanium dioxide immobilized on silica gel, J. Hazard. Mater., 152 (2008) 166–171.
[36] O.S. Lawal, A.R. Sanni, I.A. Ajayi, O.O. Rabiu, Equilibrium, thermodynamic and kinetic studies for the biosorption of aqueous lead(II) ions onto the seed husk of *Calophyllum inophyllum*, J. Hazard. Mater., 177 (2010) 829–835.
[37] W.S. Wan Ngah, S. Fatinathan, Pb(II) biosorption using chitosan and chitosan derivatives beads: equilibrium, ion exchange and mechanism studies, J. Environ. Sci., 22 (2010) 338–346.
[38] S.Y. Chen, Y. Zou, Z.Y. Yan, W. Shen, S. Shi, X. Zhang, H.P. Wang, Carboxymethylated-bacterial cellulose for copper and lead ion removal, J. Hazard. Mater., 161 (2009) 1355–1359.
[39] T. Zehra, L.B.L. Lim, N. Priyantha, Removal behavior of peat collected from Brunei Darussalam for Pb(II) ions from aqueous solution: equilibrium isotherm, thermodynamics, kinetics and regeneration studies, Environ. Earth Sci., 74 (2015) 2541–2551.
[40] K. Kalantari, M.B. Ahmad, K. Shameli, M.Z.B. Hussein, R. Khandanlou, H. Khanehzaei, Size-controlled synthesis of Fe_3O_4 magnetic nanoparticles in the layers of montmorillonite, J. Nanomater., 2014 (2014) 1–9, doi: 10.1155/2014/739485.